Vertical Phase Separation in Poly(3-hexylthiophene): Fullerene Derivative Blends and its Advantage for Inverted Structure Solar Cells

By *Zheng Xu, Li-Min Chen, Guanwen Yang, Chun-Hao Huang, Jianhui Hou, Yue Wu, Gang Li, Chain-Shu Hsu,* and *Yang Yang**

A method which enables the investigation of the buried interfaces without altering the properties of the polymer films is used to study vertical phase separation of spin-coated poly(3-hexylthiophene) (P3HT):fullerene derivative blends. X-ray photoelectron spectroscopy (XPS) and atomic force microscopy (AFM) analysis reveals the P3HT enrichment at the free (air) surfaces and abundance of fullerene derivatives at the organic/substrate interfaces. The vertical phase separation is attributed to the surface energy difference of the components and their interactions with the substrates. This inhomogeneous distribution of the donor and acceptor components significantly affects photovoltaic device performance and makes the inverted device structure a promising choice.

1. Introduction

Polymer photovoltaic (PV) cells have the advantage of low-cost fabrication and easy processing. The state-of-the-art device structure is the polymer bulk heterojunction (BHJ),[1,2] blending conjugated polymers intimately with soluble fullerene derivatives. An interpenetrating network of the donor–acceptor blend sandwiched between the anode and cathode offers large interfacial area for efficient charge separation and excellent charge transport, leading to high efficiency performance. Regioregular poly(3-hexylthiophene) (RR-P3HT) and fullerene derivative [6,6]-phenyl C_{61} butyric acid methyl ester (PCBM) blend represents one of the most promising systems. Several process conditions[3–6] and post-treatments[7,8] have been proposed to form a nano-scale phase-separated morphology with crystalline P3HT and PCBM domains, and the highest power conversion efficiency (PCE) for this system reported so far is about 4–5%.

Morphology optimization of the active layer is an essential way to improve the device efficiency. Besides the lateral phase-separated morphology, the vertical distribution of the components in the blend film is also critical, and vertical phase separation has been suggested in several polymer blend systems,[9–12] as well as P3HT:PCBM blends.[13–15] Campoy-Quiles et al. recently used variable-angle spectroscopic ellipsometry (VASE) to model the vertical composition profile of P3HT:PCBM thin films and reported a concentration gradient varying from PCBM-rich near the poly (3,4-ethylenedioxythiophene)/poly (styrene-sulfonate) (PEDOT:PSS) side to P3HT-rich adjacent to the free (air) surface. Consequently, the regular device structure (Scheme 1a), in which the polymer blend is sandwiched between the PEDOT:PSS-coated indium tin oxide (ITO) anode and low work function metal cathode, has a non-ideal composition profile. Several approaches have been proposed to modify the composition profile to achieve better device performance. For example, Campoy-Quiles et al. have shown that the compositional gradient can be switched by modifying the surface energy of the substrate with a self-assembled monolayer (SAM). Wei et al. also introduced a new fullerene derivative with a fluorocarbon chain which spontaneously forms a buffer layer near the metal cathode to improve the device performance.[16]

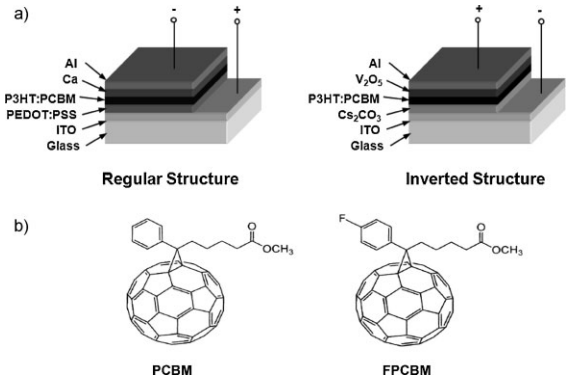

Scheme 1. a) Schematic depiction of the regular structure and inverted structure of the PV devices. b) Structures of PCBM and FPCBM.

[*] Prof. Y. Yang, Z. Xu, L.-M. Chen, G. Yang
Department of Materials Science and Engineering
University of California, Los Angeles
Los Angeles, CA 90095 (USA)
E-mail: yangy@ucla.edu
C.-H. Huang, Prof. C.-S. Hsu
Department of Applied Chemistry
National Chiao Tung University
Hsinchu, Taiwan (Republic of China)
Dr. J. Hou, Dr. Y. Wu, Dr. G. Li
Solarmer Energy, Inc.
3445 Fletcher Ave
El Monte, CA 91731 (USA)

DOI: 10.1002/adfm.200801286

As an alternative to the regular device structure (ITO/PEDOT:PSS/P3HT:PCBM/Ca/Al), the inverted device structure, e.g., [ITO/Cs_2CO_3(non-annealed)/P3HT:PCBM/V_2O_5/Al], as depicted in Scheme 1a, uses the ITO covered with a functional buffer layer as the cathode, has also been studied by several groups.[17–19] The inverted structure has the advantage of improved stability by replacing the low work function metal cathode and PEDOT:PSS, which are both detrimental to device lifetime.[20–22] It is also expected that the inverted device has the advantage over the regular configuration because of the vertical phase separation. Recently, we reported an inverted polymer solar cell by low temperature annealing of the functional Cs_2CO_3 layer.[23] The device showed 4.2% PCE under standard measurement conditions,[24] which overcame the efficiency gap between regular and inverted cells. In order to validate this assumption, detailed study of the vertical composition profile in the P3HT:PCBM blend is still necessary.

X-ray photoelectron spectroscopy (XPS) offers a useful tool for determining the composition at the sample surfaces. Unlike spectroscopic ellipsometry, in XPS the weight or molar ratio of the components can be calculated directly from the peak intensities of individual elements. However, due to the short mean free path of the photoelectrons, the probing depth of XPS is only 6–8 nm. In some cases, ion sputtering is used to investigate the concentration in bulk materials and buried interfaces.[25,26] The ion bombardment may cause various artifacts in the analysis region, e.g., chemical bonds breaking, preferential sputtering, interface mixing and phase formation or roughening, etc.[27,28] Thus, without careful calibration the concentration in the sample may differ from the depth profile.

Here, we introduce a unique method which lifts off the blend films and enables the investigation of the buried interfaces without altering film properties. In this process, a common solvent such as water is used to lift-off the blend films from various substrates and the floating films are then transferred to new conductive substrates with the selected face on the top for XPS analysis. The composition of the P3HT:PCBM blend film can be determined from the C/S atomic ratio obtained from XPS. Films spin-coated on various substrates with different procedures are studied. Furthermore, a fullerene derivative, [6,6]-(4-fluoro-phenyl)-C_{61}-butyric acid methyl ester (FPCBM), with a fluorine atom attached on the phenyl ring of PCBM (Scheme 1b) molecule, is also blended with P3HT. The attached fluorine does not alter the molecular properties significantly while providing a label for XPS analysis. Specifically, a direct comparison based on the XPS results addresses the advantage of the inverted structure over the regular one in terms of the vertical phase separation. The results are supported by corresponding atomic force microscopy (AFM) images and device characteristics. Finally, possible mechanisms which induce the vertical phase separation are also discussed.

2. Results and Discussion

2.1. XPS Analysis

The PCBM to P3HT weight ratios at the free (air) surfaces (top surface) and the organic/substrate interfaces (bottom surface) of the spin-coated films are evaluated using C/S atomic ratios obtained from the XPS measurement. O/S atomic ratios can also be used to determine the composition; however, the oxygen contamination at the sample surfaces makes the results very unreliable. For samples lifted off in water, the oxygen signals increases significantly. Since carbon is another common surface contaminant, FPCBM is used as a substituent of PCBM to evaluate the surface compositions. For samples spin-coated from P3HT:FPCBM solution, surface compositions can be directly determined from the F/S ratios without concern for the oxygen and carbon contaminations. As shown in Figure 1, the concentrations obtained from various P3HT:FPCBM sample surfaces are consistent with those acquired from their P3HT:PCBM counterparts. The results indicate that the carbon contamination at the sample surfaces is not as serious as the oxygen and the P3HT to PCBM ratios calculated from the C/S ratios are trustworthy. Moreover, the results allow us to use FPCBM to examine certain systems where it is hard to use C/S ratios to derive the P3HT to PCBM ratios, such as the polymer–PEDOT:PSS interface.

Figure 1a compares the compositions of the films spin-coated on glass substrates under four different procedures, namely fast-grown, slow-grown, fast-grown with annealing, and slow-grown

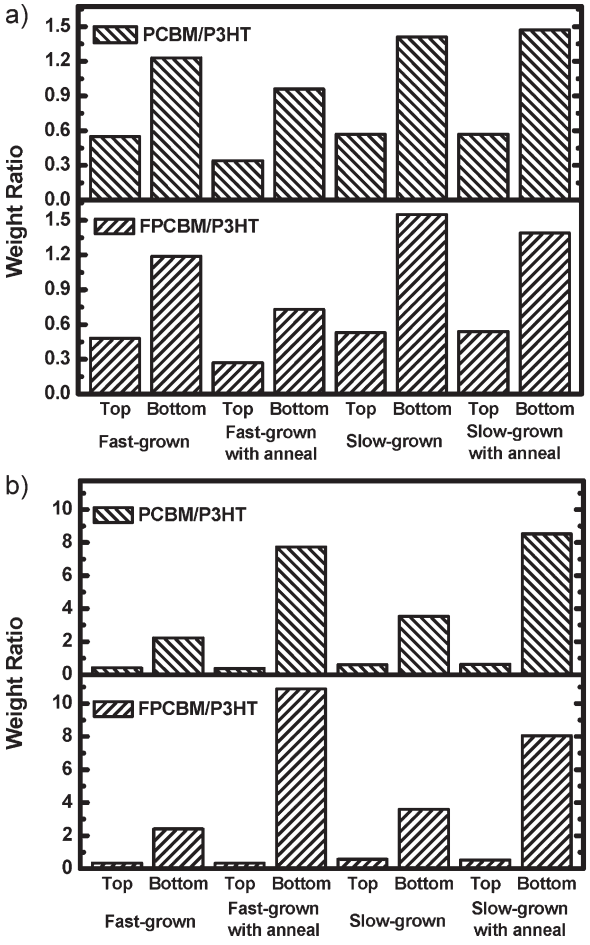

Figure 1. The compositions at the top and bottom surfaces of the blend films spin-coated on a) glass and b) Cs_2CO_3.

with annealing.[3] After lifting-off the polymer films, the glass substrates are analyzed by XPS and neither S nor F signal is detected, suggesting that the films are lifted-off entirely and no residue is left on the glass substrate. The fast-grown and slow-grown films show similar results, with higher PCBM (FPCBM) concentration at the bottom surfaces for both films. After thermal annealing, the PCBM (FPCBM) concentrations at both sides of the fast-grown films decrease slightly while the concentrations of the slow-grown films remain almost invariant. This may indicate that the fast-grown films are less thermodynamically stable.

Figure 1b illustrates the results from the films on spin-coated Cs_2CO_3. During the lift-off process, Cs_2CO_3 dissolves in water and the polymer films separate from the substrates instantaneously. The dissolution of Cs_2CO_3 is complete and no Cs signal is observed at the Cs_2CO_3 side of the films. As Figure 1b shows, the PCBM (or FPCBM) concentrations at the polymer/Cs_2CO_3 interfaces are higher than those at the polymer/glass interfaces, indicating increased vertical segregation on Cs_2CO_3 coated ITO substrates. In addition, thermal annealing further enhances this inhomogeneous distribution. The PCBM to P3HT (or FPCBM to P3HT) ratios at the Cs_2CO_3 side increase over one- and two-fold in the slow-grown and fast grown films, respectively; on the contrary, the ratios at the top surfaces only slightly decrease.

By decreasing the take-off angle (the angle between the surface of the sample and the detector) of the photoelectrons, a more near-surface composition of the polymer film can be revealed. The XPS probing depth at a take-off angle θ can be estimated as $d \sin\theta$, where d is the probing depth at 90 ° take-off angle. Further XPS studies of the fast-grown P3HT:FPCBM film with thermal annealing at a lower take-off angle (10 °) detect no F signal at the top surface and extremely weak S signals at the bottom surface. The results show a pure P3HT thin layer at the air side and an almost pure FPCBM thin layer at the Cs_2CO_3 side. Since, the S 2p and F 1s signals mainly originate from a depth of about 6 nm (the electron mean free paths are around 2 nm) at 90 ° take-off angle, the probing depth at 10 ° take-off angle is approximately 1 nm. Thus, the two layers are estimated to be 1 nm thick. Because P3HT is a hole-conducting p-type semiconductor and PCBM is an electron-conducting n-type semiconductor, this vertical inhomogeneous distribution is ideal for the previously reported inverted device structure, in which the Cs_2CO_3 layer was used as the cathode.[23] From ref.,[23] devices fabricated on annealed Cs_2CO_3 layer show a much improved performance; consequently, fast-grown P3HT:PCBM films spin-coated on 170 °C-annealed Cs_2CO_3 layer are also studied. The compositions are similar to those obtained from films spin-coated on non-annealed Cs_2CO_3, with only small decrease in the PCBM concentrations at the bottom interfaces. Other factors besides the PCBM concentration should account for the improvement of the device performance using 170 °C-annealed Cs_2CO_3, and details about I–V behavior of the devices will be discussed.

The polymer–PEDOT:PSS interface is one of the most important interfaces in polymer photovoltaic devices since in a regular device the polymer active layer is usually deposited on an ITO substrate coated with the PEDOT:PSS interfacial layer. However, the PEDOT:PSS remnant at the bottom surface of the water-lifted film hinders the elemental analysis of this interface. The PEDOT:PSS layer consists of both S and C atoms, which makes it difficult to derive the compositions in P3HT:PCBM films from the C/S ratio. Nonetheless, the compositions in P3HT:FPCBM films can instead be estimated using the F/S ratios and the compositions of the P3HT:PCBM can be inferred owing to the resemblance of the two kinds of films. Figure 2a shows the normalized S 2p peaks (containing S 2p3/2 and S 2p1/2) obtained from the top surfaces of P3HT:FPCBM films spin-coated with different procedures. The peaks at around 164 eV binding energy are assigned to the thiophene S atoms in P3HT. Small decrease in binding energy (about 0.2–0.3 eV) of the peaks are observed from the annealed samples. The F 1s and

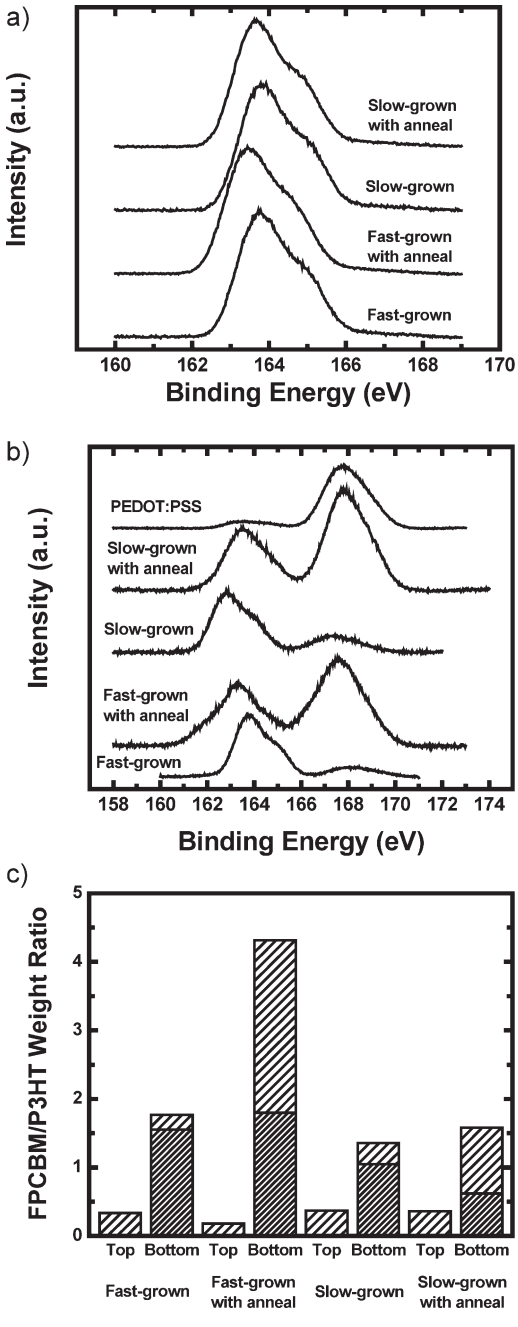

Figure 2. XPS spectra of S 2p region obtained from a) top and b) bottom surfaces of the P3HT:FPCBM films spin-coated on PEDOT:PSS. c) The composition of the films at top and bottom surfaces.

C 1s peaks from the annealed samples show almost identical shift to lower binding energies (not shown). Thus the phenomenon is unlikely caused by interactions between P3HT and FPCBM, but is induced by the change of the energy alignment at the sample/substrate interface. The S 2p peaks measured from the bottom (PEDOT:PSS) side of the P3HT:FPCBM films and from the pristine PEDOT:PSS surface are shown in Figure 2b. There are two broad peaks in the spectrum measured from the PEDOT:PSS surface. The higher (around 168 eV) and lower (around 164 eV) binding energy peaks correspond to the S atoms in the sulfonate group of PSS and in the thiophene ring of PEDOT, respectively.[29] Similarly, the S 2p spectra from the bottom side of the P3HT:FPCBM films also exhibit an additional peak at 168 eV, which comes from the remnant of PEDOT:PSS layer on the lifted films. For comparison, all the spectra from the P3HT:FPCBM films are normalized to the peak at around 164 eV while the spectrum from the PEDOT:PSS surface is normalized to the 168 eV peak. In Figure 2b, the peaks at 168 eV of the annealed films are much larger than those of the non-annealed ones, indicating more PEDOT:PSS remained at the peeled surface as well as a stronger bonding between the P3HT:FPCBM and the PEDOT:PSS layers after annealing. Figure 2c shows the FPCBM to P3HT ratios at both sides of the films estimated using F/S atomic ratios. The S 2p peak at 168 eV is not included in the calculation. (The lower part of the bars in Figure 2c shows the results incorporating the 168 eV peak.) The results indicate that the FPCBM concentrations at the PEDOT:PSS side of the films are much higher than at the top surface. In fact, the calculation still includes the S signal from the thiophene ring of PEDOT, which is also at about 164 eV. If this signal can be excluded from the calculation, the FPCBM concentration at the bottom side will be even higher. Moreover, since electrons with higher kinetic energy generally have longer mean free paths, an overlying layer diminishes the intensity of high binding energy peaks more than that of low binding energy peaks.[30] Thus, the high binding energy F 1s signal is reduced more by the remaining PEDOT:PSS layer. However, strong F 1s peaks are still observed at the bottom side of the P3HT:FPCBM films, which indicates that the remaining PEDOT:PSS layer is thin and discontinuous and the attenuation only slightly affects the results at the bottom side. The actual FPCBM concentrations at the bottom side of the films spin-coated on PEDOT:PSS are estimated to be higher than on glass but lower than on Cs_2CO_3. Similar distribution of PCBM is expected for the P3HT:PCBM films spin-coated on PEDOT:PSS layer. Consistent with the results of Campoy-Quiles et al.,[15] our findings suggest that this inhomogeneous PCBM distribution in spin-coated films are not favorable since in a regular device, ITO glass coated with PEDOT:PSS is used as the anode. Table 1 lists all the data shown in Figures 1 and 2c.

Table 1. The composition at the top and bottom surfaces of the blend films spin-coated on different substrates under various conditions.

		PCBM/P3HT (wt ratio)	FPCBM/P3HT (wt ratio)
Fast-grown	Air	0.55	0.48
	Glass	1.23	1.19
Fast-grown with anneal	Air	0.34	0.27
	Glass	0.96	0.73
Slow-grown	Air	0.57	0.53
	Glass	1.41	1.55
Slow-grown with anneal	Air	0.57	0.54
	Glass	1.47	1.39
Fast-grown	Air	0.41	0.34
	Cs_2CO_3	2.22	2.41
Fast-grown with anneal	Air	0.38	0.33
	Cs_2CO_3	7.73	10.88
Slow-grown	Air	0.60	0.58
	Cs_2CO_3	3.53	3.59
Slow-grown with anneal	Air	0.63	0.53
	Cs_2CO_3	8.53	8.05
Fast-grown	Air	–	0.34
	PEDOT:PSS	–	1.77
Fast-grown with anneal	Air	–	0.18
	PEDOT:PSS	–	4.31
Slow-grown	Air	–	0.37
	PEDOT:PSS	–	1.36
Slow-grown with anneal	Air	–	0.36
	PEDOT:PSS	–	1.58

2.2. AFM Images

AFM was also applied to evaluate the top and bottom surface composition. By rinsing the film surface with 1,8-octanedithiol (OT), which selectively dissolves PCBM,[31] the polymer network can be exposed, allowing the qualitative evaluation of the relative compositions. Figure 3 shows the height and phase images of the exposed top and bottom surfaces of fast grown films spin-coated on glass substrate. Prior to exposing the polymer network, the top and bottom surfaces show similar smooth films (not shown), which do not show a clear indication of the individual components. However, after selectively dissolving away the fullerene phase by OT, the difference between the exposed polymer network of the top and bottom surfaces is obvious (Fig. 3). The bottom surface clearly shows a much larger surface roughness ($R_q = 6.9$ nm, compared to $R_q = 1.03$ nm for the top surface), and the phase image shows a much larger contrast, indicating the existence of more fullerene phase, consistent with the XPS results.

2.3. Device Properties

The XPS and AFM results suggest the advantage of the inverted device structure over the regular one. A concentration distribution with PCBM-rich near the cathode and P3HT-rich adjacent to the anode can be expected to improve the short circuit current (J_{SC}). For fast-grown devices without annealing, the morphology of the active layer is not optimized, thus both the inverted and regular structures show similar performances of PCE < 1%, hindering the differences of these two configurations. Annealing the P3HT:PCBM (or P3HT:FPCBM) active layer (at 110 °C for 10 min) enhanced the phase separation and crystallinity of the P3HT chains, leading to significant improvement in device performance. Moreover, pre-annealing increases the vertical segregation and the advantage of the inverted structure over the regular structure is apparent under the same spin-coating

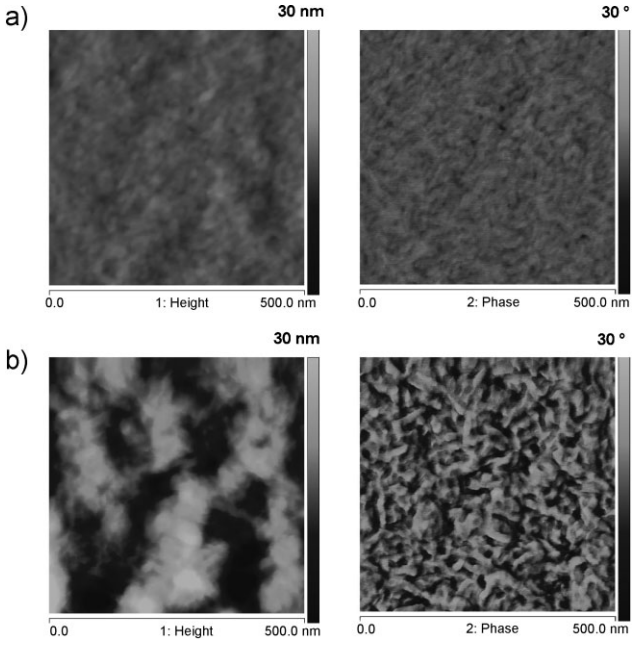

Figure 3. AFM topography (left) and phase (right) images of a) top and b) bottom surfaces of the exposed P3HT networks. The PCBM in the fast grown blend films spin-coated on glass was selectively removed using OT.

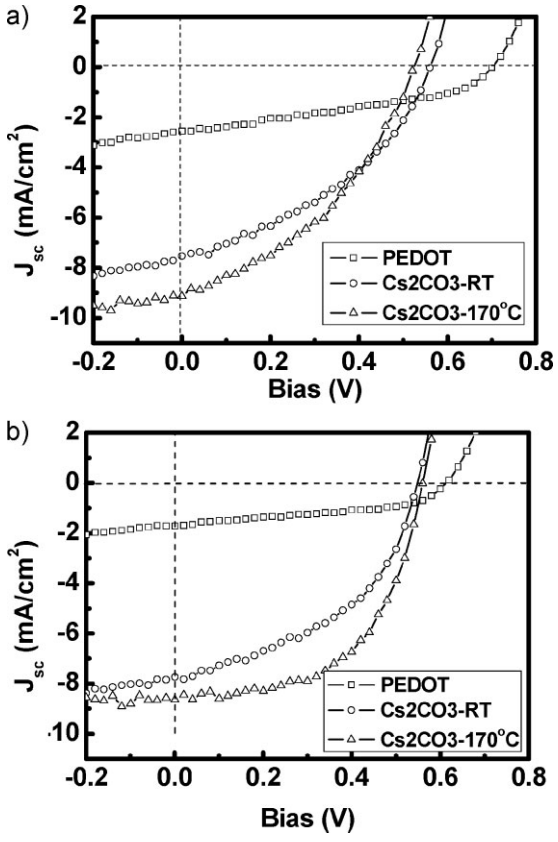

Figure 4. *J–V* characteristics under illumination for pre-annealed fast-grown a) P3HT:PCBM and b) P3HT:FPCBM photovoltaic devices with different structure.

parameters. For the P3HT:PCBM devices, as illustrated in Figure 4a, a three-fold increase in J_{SC} (2.61–7.53 mA cm^{-2}) is obtained for the inverted device. If the 170 °C-annealed Cs_2CO_3 is incorporated in the inverted structure, the device efficiency tripled to 2%, with even higher J_{SC} (9.13 mA cm^{-2}). For the P3HT:FPCBM devices, as shown in Figure 4b, the improvement is even more significant, with an almost five-fold increase in J_{SC} (1.82 vs. 8.64 mA cm^{-2}) and PCE (0.56 vs. 2.70%). As mentioned earlier, the annealed Cs_2CO_3 does not further increase the vertical phase separation. The J_{SC} improvement is due to a lower interfacial resistance contact formed upon Cs_2CO_3 annealing.[23] The series resistance for the non-annealed Cs_2CO_3 devices and the 170 °C-annealed Cs_2CO_3 devices are only a fraction of the regular ones, indicating the reduced resistivity of the interface. This series resistance reduction can be attributed to an improved interface morphology, since for the inverted devices, the Cs_2CO_3 side (cathode) is PCBM-rich, while the opposite V_2O_5/Al side (anode) is P3HT-rich, and thus charge carrier recombination can be substantially reduced. The detailed device operational parameters are summarized in Table 2.

The external quantum efficiency (EQE) results obtained from the P3HT:PCBM devices are shown in Figure 5. The inverted device structure clearly shows a higher EQE over the entire solar spectrum, with a maximum of 64% at 514 nm, which corresponds to the significantly higher J_{SC} compared to the regular device structure. Despite the higher EQE on the non-annealed Cs_2CO_3 films, the J_{SC} is lower due to a higher interface resistance of the pristine Cs_2CO_3 layer itself. The interesting part is the substantial EQE contribution from the PCBM (~350 nm), which is not seen for the regular device structure, even for a slow-grown device.[3] Since the UV–Vis absorption results (not shown here) show no distinct differences between the regular and inverted device structure, this increased EQE can be attributed to the accumulation of the electron acceptor material at the cathode due to self-stratification, which may lead to a more efficient charge collection. This excess EQE contribution from PCBM validates

Table 2. Short-circuit current density ($J_{<sub>SC}$), open-circuit voltage (Voc), PCE, and fill factor (FF) of various photovoltaic devices shown in Figures 4 and 5.

		Voc [V]	Jsc [mA cm^{-2}]	FF [%]	PCE [%]	Rs [Ω cm^{-2}]
P3HT:PCBM	PEDOT:PSS	0.68	−2.61	0.74	41.48	7.19
	Cs_2CO_3 (RT)	0.56	−7.53	1.69	40.14	2.58
	Cs_2CO_3 (170 °C)	0.52	−9.13	1.93	40.59	0.98
P3HT:FPCBM	PEDOT:PSS	0.60	−1.82	0.56	50.77	12.62
	Cs_2CO_3 (RT)	0.54	−7.74	1.94	46.43	3.35
	Cs_2CO_3 (170 °C)	0.56	−8.64	2.70	55.69	2.25

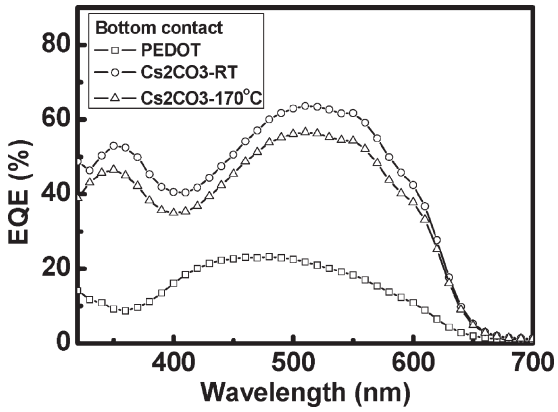

Figure 5. EQE results obtained from the pre-annealed fast-grown P3HT:PCBM devices.

the advantage of the vertical phase separation for the inverted structure.

Other processed and treatments like slow-grown film followed by thermal annealing can further improve the lateral phase-separated morphology and lead to better device performance. Meanwhile, the vertical composition distribution does not vary significantly. As a result, the effects related to the vertical phase separation become obscure. The best regular P3HT:PCBM device fabricated in our lab so far has the efficiency of 4.4%, which is slightly higher than our newly-reported inverted device structure with 4.2% PCE. However, the inverted device still benefited from this vertical phase separation, with a higher EQE maximum (72% compared to 63%) and a higher J_{SC} (11.13 vs. 10.6 mA cm^{-2}). Furthermore, the non-negligible optical loss from the PEDOT:PSS layer may also account the improvement in the inverted devices.[32] Further performance improvement of the inverted devices can be expected by optimizing the energy alignment at the polymer/electrode interfaces and improving the conductivity of the functional buffer layers.

2.4. Formation of the Vertical Phase Separation

The vertical phase separation in the polymer blend is believed to be related to the differences in the surface energy of each component. Since P3HT has a lower surface energy than PCBM, it tends to accumulate at the air surface in order to reduce the overall energy.[10,34] The solvent evaporation process during spin-coating allows the morphology to reach a thermodynamically favorable state via vertical phase separation. This similar surface enrichment phenomenon has also been observed in other polymer blend systems, such as the multilayer structure formed in the APFO-3/PCBM (1:4) film, with surface enrichment of APFO-3[10] and enrichment of the lower surface energy component TFB at the surface for TFB/F8BT blend,[33] as well as a partially crystallized wetting layer formed by the polyfluorene (PFO) for PFO/F8BT blend.[34]

Due to the hydrophilic nature of the non-annealed Cs_2CO_3 layer, PCBM tends to accumulate much stronger on Cs_2CO_3 than on glass substrates. PCBM itself has a very high density of electrons, thus the resulting induced dipole moments presumably affect the intermolecular interactions between the PCBM molecules. Ohno et al. suggested an enhanced intermolecular interaction due to the dipole field created by the induced dipole moments in C_{60} overlayers, which was caused by strong charge transfer from the substrate to the first-layer C_{60} molecules.[35] It is expected that PCBM and FPCBM should behave similarly to C_{60} in this aspect. Indeed, our XPS results show a significant binding energy shift (~0.5 eV) to lower binding energy for Cs after spin-coating an ultra-thin PCBM layer above, suggesting substantial charge transfer. We have previously demonstrated that the spin-coated Cs_2CO_3 layer forms a strong dipole on the ITO substrate,[36] thus induced dipole–dipole interaction should also contribute to the accumulation of PCBM at the polymer/Cs_2CO_3 interface. For the 170 °C-annealed Cs_2CO_3 layer, the surface becomes less hydrophilic,[23] thus only charge transfer contributes to the weaker affinity for PCBM accumulation. Glass substrates have a relatively hydrophobic surface before UV-ozone treatment, and are not preferable for PCBM accumulation. From our results, both surface energy and charge transfer play a role in the PCBM accumulation on various substrates, and further studies are undergoing to elucidate the detailed mechanism of the vertical phase separation.

The most significant PCBM accumulation occurs after pre-annealing the polymer film on non-annealed Cs_2CO_3 layer, which is due to the strongest dipole–dipole interaction. This even stronger PCBM segregation after annealing is because the spin-coated film has an intermediate morphology after spin-coating, and the annealing process provides the driving force for the polymer film to achieve a more thermodynamically favorable morphology. It has been suggested that if thermal equilibrium is reached, a bilayer structure should form eventually.[10]

If the vertical segregation can be controlled to a desired morphology, where the cathode is acceptor-enriched and the anode is donor-enriched, efficient charge dissociation via the interpenetrating network and efficient charge transport along the interconnected pathway, as well as efficient charge collection at the interface can substantially enhance the device performance. This favorable morphology based on the vertical segregation is depicted in Scheme 2. Nonetheless, Khodabakhsh et al. have shown that changes in surface wettability influences how the subsequently deposited organic molecules assemble and orient themselves, thus affecting the density of available charge collection sites in organic solar cells.[37] As a consequence, a PCBM-rich layer at the Cs_2CO_3 interface is beneficial and would improve the device performance for the inverted configurations.

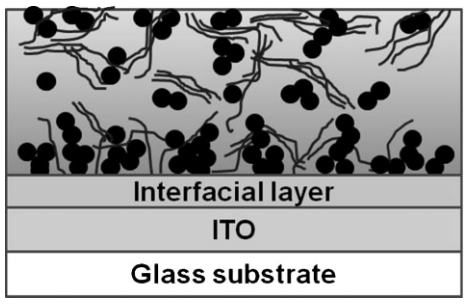

Scheme 2. Schematic of the vertical phase separation of the polymer: fullerene blend.

3. Conclusions

As a conclusion, we introduced a unique method which enables the investigation of the buried interfaces without altering the polymer film properties. Detailed XPS analysis provided an insight to the interfaces of the polymer/substrate, revealing spontaneous vertical stratification upon spin-coating the polymer films, as well as the enrichment of the donor and acceptor components at the top and bottom surfaces, respectively. This vertical phase separation is attributed to the differences in surface energy and induced dipole–dipole interactions between PCBM and the substrates. By varying the surface property of the substrate, the distribution of the donor and acceptor materials can be manipulated, and the consequent vertical phase separation makes the inverted structure a promising choice for polymer solar cells.

4. Experimental

The device structures of regular and inverted polymer solar cells are illustrated in Scheme 1a. The ITO substrates were pre-cleaned and treated with UV-ozone for 15 min prior to spin-coating. The regular device structure consists of an ITO substrate coated with a PEDOT:PSS interfacial layer as the anode; Ca (20 nm) and Al (80 nm) were thermally-evaporated as the cathode. For the inverted structure, 0.2 wt % Cs_2CO_3 was dissolved in 2-ethoxyethanol and spin-coated on ITO substrates at 3000 rpm to function as the cathode. Some of these Cs_2CO_3 covered cathodes were annealed at 170 °C for 20 min inside the glove box before depositing the polymer active layer, and the surface property of this cathode layer can be manipulated by thermal annealing treatment. V_2O_5 (10 nm) and Al (800 nm) were thermally-evaporated as the anode for the inverted devices. RR-P3HT and PCBM (or FPCBM) were separately dissolved in 1, 2 dichlorobenzene (DCB) and blended together in a 1:1 w/w ratio to form a 2 wt % solution. In order to exclude the possible effect of PCBM distribution from slow growth, the active layers were spin-coated at 2000 rpm for 90 s, and were completely dried, visualized from the red-purplish color after spin coating. Preannealing was carried out inside the glove box at 110 °C for 10 min before electrode evaporation. Device testing was performed following the rules of ref. [24] and under simulated AM1.5G irradiation (100 mW cm^{-2}) using a xenon-lamp-based solar simulator (Oriel 96000 150W Solar Simulator).

The samples for XPS analysis were prepared using the same P3HT:PCBM and P3HT:FPCBM blend solutions. The polymer films were spin-coated on bare glass substrates or substrates pre-coated with PEDOT:PSS or Cs_2CO_3 buffer layers. The Cs_2CO_3 was spin-coated on glass at 1000 rpm for 60 s to ensure full coverage over the glass surface while the PEDOT:PSS layer was spin-coated at the same condition as the device fabrication. The polymer films were prepared using four different procedures, namely fast-grown (3000 rpm, 60 s), slow-grown (800 rpm, 40 s with solvent annealing), fast-grown with annealing (thermal annealing at 110 °C for 10 min) and slow-grown with annealing (thermal annealing 110 °C for 10 min).

During the lift-off process, the spin-coated polymer film was pre-cut into several small pieces and rinsed in water. For samples spin-coated on the glass substrates, due to the different surface energy between the glass substrate and the polymer layer, water delaminates the polymer film from the substrate. For samples spin-coated on Cs_2CO_3 or PEDOT:PSS buffer layers, the P3HT:PCBM (or P3HT:FPCBM) films detach from the substrates because of the water-soluble Cs_2CO_3 or PEDOT:PSS buffer layers. As a result, the small pieces of P3HT:PCBM (or P3HT:FPCBM) films were lifted off and floated on the water with the free (air) surface on top. Then the ''lifted-off'' films were transferred to Ag coated Si substrates with selected surface on top.

Because P3HT and PCBM (or FPCBM) are insoluble in water, immersing in water does not change the PCBM to P3HT (or FPCBM to P3HT) ratios. In another experiment, the top surfaces of the films were treated carefully with water (without peeling off the organic film from the substrate), but no variations in the PCBM to P3HT ratio were observed before and after the water treatment. Due to adsorption of the hydroxyl groups, the oxygen signals from the surfaces contacted with water were much stronger. However, since the oxygen signals were not used in the calculation, rinsing in water did not affect our results.

The XPS measurements were performed inside an Omicron XPS/UPS system. The base pressure in the analysis chamber of the system was better than 10^{-9} mbar. A monochromatic Al Kα (1486.6 eV) X-ray source was used for excitation and the spectra were collected with a pass energy of 50 eV.

The atomic ratios were evaluated using the following equation:

$$\frac{n_1}{n_2} = \frac{I_1/S_1}{I_2/S_2} \quad (1)$$

where I is the peak area and S is the atomic sensitivity factor. The integrated areas of the XPS peaks were calculated using XPSPEAK41software and the Shirley method was used to subtract the background. The atomic sensitivity factors were extracted from the empirical values reported by Wagner et al.[38]. Due to different instrumental design, the sensitivity factors of different systems may not be the same. However, the accuracy of our results can be evaluated using the following method.

Since the carbon contamination at the sample surfaces is negligible, the S/C and F/C atomic ratios in P3HT-only and FPCBM-only samples should be close to stoichiometry. The sensitivity factors of the S, C, and F elements can thus be calculated by comparing the intensities of corresponding XPS peaks. The C/S and F/S atomic ratios calculated using these sensitivity factors are 13 and 17% lower than using values from [38], respectively. As a result, the FPCBM to P3HT ratios are 17% lower than the values shown in Table 1, while the PCBM to P3HT ratios are 15–25% lower at the bottom surface and 30–40% lower at the top surface. The ratio differences are acceptable and do not affect any conclusion in this paper.

Fast grown P3HT:PCBM films on glass substrates were used for AFM imaging. P3HT network films were prepared by rinsing the P3HT:PCBM film with OT for several seconds. In order to observe the organic/glass interface of the sample, P3HT:PCBM films were peeled off using water and transferred to another glass substrate with the bottom side up before the OT treatment. The AFM images were obtained with tapping mode AFM (Nanoscope IIIa, Veeco Instruments).

Acknowledgements

Z. Xu and L.-M. Chen contributed equally to this work. The authors gratefully acknowledge financial support from Solarmer Inc., University of California Discovery Grant, and NSF IGERT: Materials Creation Training Program (MCTP) (DGE-0114443) and the California Nano-Systems Institute. The authors also thank Dr. H.-H. Liao, Dr. S. H. Li, Dr. Y. Yao, W. L. Kwan, and V. Tung for their fruitful discussions.

Received: August 30, 2008
Published online: March 13, 2009

[1] G. Yu, J. Gao, J. C. Hummelen, F. Wudl, A. J. Heeger, *Science* **1995**, *270*, 1789.
[2] J. J. M. Halls, C. A. Walsh, N. C. Greenham, E. A. Marseglia, R. H. Friend, S. C. Moratti, A. B. Holmes, *Nature* **1995**, *376*, 498.
[3] G. Li, V. Shrotriya, J. Huang, Y. Yao, T. Moriarty, K. Emery, Y. Yang, *Nat. Mater.* **2005**, *4*, 864.
[4] G. Li, V. Shrotriya, Y. Yao, J. Huang, Y. Yang, *J. Mater. Chem.* **2007**, *17*, 3126.
[5] S. E. Shaheen, C. J. Brabec, N. S. Sariciftci, F. Padinger, T. Fromherz, J. C. Hummelen, *Appl. Phys. Lett.* **2001**, *78*, 841.

[6] G. Li, Y. Yao, H. Yang, V. Shrotriya, G. Yang, Y. Yang, *Adv. Funct. Mater.* **2007**, *17*, 1636.
[7] Y. Kim, S. A. Choulis, J. Nelson, D. C. Bradley, S. Cook, J. R. Durrant, *Appl. Phys. Lett.* **2005**, *86*, 063502.
[8] W. Ma, C. Yang, X. Gong, K. Lee, A. J. Heeger, *Adv. Funct. Mater.* **2005**, *16*, 1617.
[9] S. Goffri, C. Müller, N. Stingelin-Stutzmann, D. W. Breiby, C. P. Radano, J. W. Andreasen, R. Thompson, R. A. J. Janssen, M. M. Nielsen, P. Smith, H. Sirringhaus, *Nat. Mater.* **2006**, *5*, 950.
[10] C. M. Björström, A. Bernasik, J. Rysz, A. Budkowski, S. Nilsson, M. Svensson, M. R. Andersson, K. O. Magnusson, E. Moons, *J. Phys.: Condens. Matter* **2005**, *17*, L529.
[11] R. A. L. Jones, L. J. Norton, E. J. Kramer, F. S. Bates, P. Wiltzius, *Phys. Rev. Lett.* **1991**, *66*, 1326.
[12] A. M. Higgins, S. J. Martin, R. L. Thompson, J. Chappell, M. Voigt, D. G. Lidzey, R. A. L. Jones, M. Geoghegan, *J. Phys. : Condens. Matter* **2005**, *17*, 1319.
[13] M. Reyes-Reyes, K. Kim, J. Dewald, R. López-Sandoval, A. Avadhanula, S. Curran, D. L. Carroll, *Org. Lett.* **2005**, *7*, 5749.
[14] C. Waldauf, M. Morana, P. Denk, P. Schilinsky, K. Coakley, S. A. Choulis, C. J. Brabec, *Appl. Phys. Lett.* **2006**, *89*, 233517.
[15] M. Campoy-Quiles, T. Ferenczi, T. Agostinelli, P. G. Etchegoin, Y. Kim, T. D. Anthopoulos, P. N. Stavrinou, D. C. Bradley, J. Nelson, *Nat. Mater.* **2008**, *7*, 158.
[16] Q. Wei, T. Nishizawa, K. Tajima, K. Hashimoto, *Adv. Mater.* **2008**, *20*, 1.
[17] G. Li, C.-W. Chu, V. Shrotriya, J. Huang, Y. Yang, *Appl. Phys. Lett.* **2006**, *88*, 253503.
[18] M. S. White, D. C. Olson, S. E. Shaheen, N. Kopidakis, D. S. Ginley, *Appl. Phys. Lett.* **2006**, *89*, 143517.
[19] R. Steim, S. A. Choulis, P. Schilinsky, C. J. Brabec, *Appl. Phys. Lett.* **2008**, *92*, 093303.
[20] Y. Sahin, S. Alem, R. de Bettingnies, J. M. Nunzi, *Thin Solid Films* **2005**, *476*, 340.
[21] A. Watanabe, A. Kasuya, *Thin Solid Films* **2005**, *483*, 358.
[22] M. P. de Jong, L. J. van Ijzendoom, M. J. A. de Voigt, *Appl. Phys. Lett.* **2000**, *77*, 2255.
[23] H.-H. Liao, L.-M. Chen, Z. Xu, G. Li, Y. Yang, *Appl. Phys. Lett.* **2008**, *92*, 173303.
[24] V. Shrotriya, G. Li, Y. Yao, T. Moriarty, K. Emery, Y. Yang, *Adv. Funct. Mater.* **2006**, *16*, **2016**.
[25] M. Kwoka, L. Ottaviano, M. Passacantando, S. Santucci, J. Szuber, *Appl. Surf. Sci.* **2006**, *252*, 7730.
[26] W. Song, S. K. So, J. Moulder, Y. Qiu, Y. Zhu, L. Cao, *Surf. Interface Anal.* **2001**, *32*, 70.
[27] S. G. MacKay, M. Bakir, I. H. Musselman, T. J. Meyer, R. W. Linton, *Anal. Chem.* **1991**, *63*, 60.
[28] A. Turak, D. Grozea, X. D. Feng, Z. H. Lu, H. Aziz, A. M. Hor, *Appl. Phys. Lett.* **2002**, *81*, 766.
[29] J. Hwang, F. Amy, A. Kahn, *Org. Electr.* **2006**, *7*, 387.
[30] J. F. Moulder, W. F. Stickle, P. E. Sobol, K. D. Bomben, in *Handbook of X-ray Photoelectron Spectroscopy* (Eds: J. Chastain, R. C. King, Jr,) Physical Electronics, Inc, United States **1995**.
[31] J. K. Lee, W. L. Ma, C. J. Brabec, J. Yuen, J. S. Moon, J. Y. Kim, K. Lee, G. C. Bazan, A. J. Heeger, *J. Am. Chem. Soc.* **2008**, *130*, 3619.
[32] T. Ameri, G. Dennler, C. Waldauf, P. Denk, K. Forberich, M. C. Scharber, C. J. Brabec, K. Hingerl, *J. Appl. Phys.* **2008**, *103*, 084506.
[33] J. S. Kim, P. K. H. Ho, C. E. Murphy, R. H. Friend, *Macromolecule* **2004**, *37*, 2861.
[34] S. Y. Heriot, R. A. L. Jones, *Nat. Mater.* **2005**, *4*, 782.
[35] K. Ohno, Y. Kawazoe, *Scr. Mater.* **2001**, *44*, 1579.
[36] J. Huang, G. Li, Y. Yang, *Adv. Mater.* **2008**, *20*, 415.
[37] S. Khodabakhsh, B. M. Sanderson, J. Nelson, T. S. Jones, *Adv. Funct. Mater.* **2006**, *16*, 95.
[38] C. D. Wagner, L. E. Davis, M. V. Zeller, J. A. Taylor, R. H. Raymond, L. H. Gale, *Surf. Interface Anal.* **1981**, *3*, 211.